

# Monsoon-influenced variation of clay mineral compositions and detrital Nd-Sr isotopes in the western Andaman Sea (IODP Site U1447) since the late Miocene

Jongmin Lee<sup>a,1</sup>, Sunghan Kim<sup>b,1</sup>, Jae Il Lee<sup>b</sup>, Hyen Goo Cho<sup>c</sup>, Stephen C. Phillips<sup>d</sup>,  
Boo-Keun Khim<sup>a,\*</sup>

<sup>a</sup> Department of Oceanography, Pusan National University, Busan 46241, South Korea

<sup>b</sup> Division of Polar Paleoenvironment, Korea Polar Research Institute, Incheon 21990, South Korea

<sup>c</sup> Department of Geology and Research Institute of Natural Science, Gyeongsang National University, Jinju 52828, South Korea

<sup>d</sup> Institute for Geophysics, Jackson School of Geosciences, University of Texas at Austin, Austin, TX 78712, USA

## ARTICLE INFO

### Keywords:

Provenance  
Weathering intensity  
Indian monsoon  
Paleoclimate

## ABSTRACT

Nd-Sr isotopes ( $\epsilon_{\text{Nd}}$ ,  $^{87}\text{Sr}/^{86}\text{Sr}$ ) of detrital particles, clay mineral compositions, and  $\delta^{13}\text{C}$  of sediment organic matter ( $\delta^{13}\text{C}_{\text{SOM}}$ ) at the International Ocean Discovery Program (IODP) Expedition 353 Site U1447 in the western Andaman Sea were measured to reveal the sediment provenance changes and/or weathering intensity variations in association with the Indian monsoon intensity change. The shipboard age model based on biostratigraphic data and paleomagnetic reversals shows that IODP Site U1447 preserves late Miocene (~10 Ma) sediments. Nd/Sr isotope systematics demonstrates that the sediments originated mainly from the Myanmar region, including the Irrawaddy River, Salween River, Sittang River and Indo-Burman-Arakan Ranges without a significant change of sediment provenance since the late Miocene. Thus, temporal variations of clay mineral compositions, represented as smectite/(illite + chlorite) [S/(I + C)], indicate the long-term variations of physical/chemical weathering intensity attributable to intensity changes of Indian winter/summer monsoon. A gradual decreasing trend of S/(I + C) ratios indicates stronger physical and/or weaker chemical weathering since the late Miocene, as a result of strengthening of Indian winter monsoon (and/or weakening of Indian summer monsoon), which seems to be closely related to global cooling since the late Miocene. Distinct decrease of S/(I + C) ratios occurred at ~9.2–8.5 Ma, ~3.6 Ma, ~2.4 Ma, and ~1.2 Ma, which may be attributed to the combined effect of both global cooling and Tibetan Plateau Uplift as a local response. In addition,  $\delta^{13}\text{C}_{\text{SOM}}$  values at IODP Site U1447 were higher at ~3.5 Ma and after 1.5 Ma when S/(I + C) ratio was minima, which may imply an increase of  $\text{C}_4$  plant in Myanmar region as a result of the strong Indian winter monsoon (or weak Indian summer monsoon).

## 1. Introduction

The Asian monsoon systems are composed of the South Asian monsoon, also known as the Indian monsoon, and the East Asian monsoon, both of which have a dominant influence on Asian continental climate. The evolution of these monsoons has played an important role in understanding global and regional climate change (Wang et al., 2003). The Indian monsoon primarily affects neighboring continental regions, including the Himalayas, Peninsular India, Myanmar, and the Malay Peninsula, whereas the East Asian monsoon influences mainly China and East Asian countries, including Korea and Japan. These monsoon systems consequently affect human societies and environmental conditions.

Many studies suggest that the Indian and East Asian monsoons have

developed similarly since the Miocene (e.g., An et al., 2001; Wan et al., 2010). Wan et al. (2010) reported reducing intensity of the East Asian summer monsoon since the early Miocene (~20 Ma), based on minimal chemical weathering at the International Ocean Discovery Program (IODP) Site 1146 in the South China Sea. Clift et al. (2008) also suggested weakened intensity of the Indian summer monsoon since the middle Miocene (~17 to 15 Ma) based on decreased chemical index of alteration (CIA) from a core (Indus Marine A1) located offshore the Indus Delta in the Arabian Sea. However, unsolved questions still remain concerning the evolution of these monsoon systems in the geologic (long-term) time-scale. For example, some studies suggested that the intensity of the Indian monsoon increased from the late Miocene to the Pliocene (e.g., An et al., 2001). In contrast, other studies reported that its strength might have decreased during the

\* Corresponding author.

E-mail address: [bkkhim@pusan.ac.kr](mailto:bkkhim@pusan.ac.kr) (B.-K. Khim).

<sup>1</sup> Equally contributed author.

same period (e.g., Clift et al., 2008; Tripathi et al., 2017).

Although the Andaman Sea sensitively responds to Indian monsoon variation, studies on its long-term paleo-monsoon records are relatively limited, compared to those that focus on the neighboring Arabian Sea and Bay of Bengal (Gupta et al., 2015; Tripathi et al., 2017). Several investigations have been recently conducted to reveal variations of Indian monsoon strength in the Andaman Sea (Colin et al., 1999, 2006; Ali et al., 2015; Sijinkumar et al., 2016; Miriyala et al., 2017; Gebregiorgis et al., 2018). However, most of these studies are limited to the penultimate glacial-interglacial period. For example, Miriyala et al. (2017) reported different chemical weathering intensity in the drainage basin of the Irrawaddy River between the Holocene and the last glacial period, attributed to changes in the monsoon strength. Gebregiorgis et al. (2018) analyzed the longest orbital-scale record to date from NGHP Site 17 and used sea-surface temperature and seawater  $\delta^{18}\text{O}$  records over the last 1 Myr to show Southern Hemisphere influence on monsoon intensity. According to tectonic time-scale investigations from NGHP Site 17 in the western Andaman Sea, Phillips et al. (2014) reported long-term changes in clay mineral composition, Johnson et al. (2014) reported long-term variation in organic carbon,  $\text{CaCO}_3$ , and  $\delta^{13}\text{C}$  of organic matter, and Cawthern et al. (2014) found long-term variation in biogenic silica paleoproductivity. However, the interpretations of past monsoon variability in these studies were limited by a Pliocene hiatus in sedimentation (Flores et al., 2014).

Variability in monsoon strength plays an important role in low-latitude

local/regional climate (Webster, 1987). Moreover, monsoon-derived precipitation is a dominant contributor to weathering and erosion in continental regions (Derry and France-Lanord, 1996; Clift et al., 2008). Due to increased seasonal precipitation, the input of terrigenous sediments from continental to marine environments is greater during the Indian summer monsoon season. Thus, deposition of terrigenous sediments in the deep-sea environment can preserve the weathering and erosion history in potential source regions, driven by variations in the Indian monsoon (e.g., Colin et al., 1999, 2006). In this paper, we report clay mineral compositions of fine-grained sediments, neodymium (Nd) and strontium (Sr) isotope measurements of detrital particles, and  $\delta^{13}\text{C}$  of sediment organic matter (SOM) ( $\delta^{13}\text{C}_{\text{SOM}}$ ) using samples from IODP Expedition 353 Site U1447 in the western Andaman Sea. The main goal of this study is to reveal sediment provenance and weathering intensity since the late Miocene to better understand the long-term evolution of the Indian monsoon in the western Andaman Sea.

## 2. Study area

### 2.1. Geological and oceanographic setting in the Andaman Sea

The Andaman Sea is a semi-enclosed basin surrounded by the Malay Peninsula, Sumatra Island, and the Andaman Islands (Fig. 1a). The Andaman-Sumatra island arc system was formed by oblique subduction

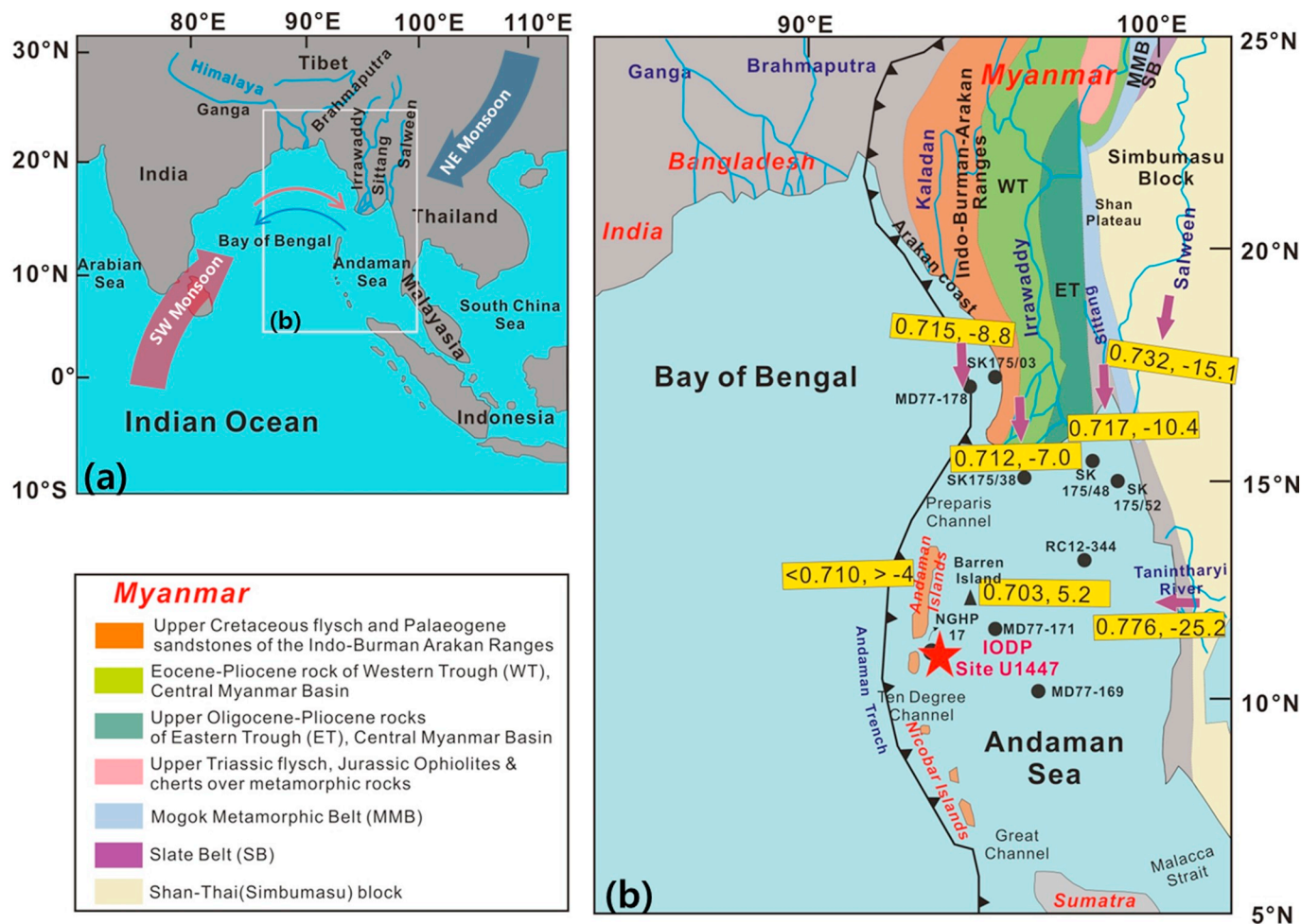


**Fig. 1.** (a) The study area including the Bay of Bengal and the Andaman Sea with major rivers (Ganga River, Brahmaputra River, Irrawaddy River, Salween River, and Sittang River) influenced by the Indian monsoon with seasonal wind and surface current (red: summer, blue: winter). (b) Lithologic map of river drainage basins in the Myanmar region and representative ( $^{87}\text{Sr}/^{86}\text{Sr}$  and  $\epsilon_{\text{Nd}}$ ) of end-members (Indo-Burma-Arakan (IBA) Ranges, Irrawaddy River, Salween River, Sittang River, Tanintharyi River, Andaman Island, and Barren Island; Colin et al., 1999; Luhr and Haldar, 2006; Awasthi et al., 2014; Damodararao et al., 2016; Miriyala et al., 2017; Giosan et al., 2018), the location of cores cited in the text (Colin et al., 1999; Ali et al., 2015; Miriyala et al., 2017) and IODP Site U1447 in the Andaman Sea. (For interpretation of the references to color in this figure legend, the reader is referred to the web version of this article.)

of the Indo-Australian plate beneath the Eurasian plate (Singh et al., 2013). Stretching and rifting of the overriding plate during the early Miocene (~25 Ma) caused separation of Sunda and Burma plates by active spreading, resulting in the formation of the Andaman Sea (Curry, 2005). The Andaman Sea is separated from the Bay of Bengal to the west by the Andaman-Nicobar Islands. Seawater exchange with the Bay of Bengal is limited through the Preparis Channel, the Ten Degree Channel, and the Great Channel (Fig. 1b). The Malacca Strait to the south connects the Andaman Sea to the South China Sea (Fig. 1a).

The Andaman Sea is characterized by seasonal monsoon variation, which results in reversing surface circulation controlling the dispersal and deposition of terrigenous sediments in the Andaman Sea (Rizal et al., 2012). During the summer monsoon (Southwest monsoon; SW), the direction of surface current is cyclonic, whereas anti-cyclonic current is dominant during the winter monsoon (Northeast monsoon; NE) (Potemra et al., 1991). Moreover, during the SW monsoon, a great amount of terrigenous sediments and freshwater was supplied to the Andaman Sea by river systems of Myanmar region, and > 80% of annual rainfall, runoff, and terrigenous sediment discharge occur during this period (Rao et al., 2005).

## 2.2. Potential sediment source regions to the Andaman Sea

The principal sources of sediments to the Andaman Sea are known as the Irrawaddy River, Salween River, and Sittang River in the Myanmar region (Awasthi et al., 2014; Ali et al., 2015; Miriyala et al., 2017), which supply in total > 550 million tons of sediments annually (Miriyala et al., 2017) (Fig. 1b). In addition, the western Myanmar region (i.e., the Indo-Burman-Arakan (IBA) Ranges) are also constitutes the sediment source through a moderately small river such as Kaladan River (Kurian et al., 2008; Garzanti et al., 2016). Recently, the Western Thailand area is also suggested as one of the potential source regions to supply sediments to the Andaman Sea through the small river (i.e., Tanintharyi River) (Damodararao et al., 2016). However, the accurate sediment flux information of these regions (i.e., IBA Ranges and Western Thailand) has not been reported yet. Finally, the Andaman Island and small volcanic Islands such as the Barren Island have played an additional local sediment source (Fig. 1b). Thus, in this study, we considered the possible six sediment provenances (Irrawaddy River, Salween River, Sittang River, IBA Ranges, Western Thailand, and the Andaman volcanics) to the western Andaman Sea. Although Ganges-Brahmaputra River system has played additional sediment source to the Andaman Sea, we disregard these river systems because sediment contribution to the study area seems relatively minor (Colin et al., 1999).

The sediments derived from the different source regions record the specific values of radiogenic isotopes (e.g., Nd and Sr) due to the different lithologies of drainage basins (Awasthi et al., 2014; Damodararao

et al., 2016; Giosan et al., 2018; references therein). Table 1 summarizes the average  $\epsilon_{Nd}$  value and  $^{87}Sr/^{86}Sr$  ratio for the possible end-members of sediment provenances based on the published available data. Giosan et al. (2018) reported that  $\epsilon_{Nd}$  values and  $^{87}Sr/^{86}Sr$  ratios of the Irrawaddy River sediments vary from  $-7.3$  to  $-6.8$  (av.  $-7.0$ ) and from  $0.7118$  to  $0.7120$  (av.  $0.7119$ ), respectively. In contrast, average  $\epsilon_{Nd}$  value and  $^{87}Sr/^{86}Sr$  ratio of the Sittang River sediments are  $-10.4$  and  $0.7168$ , respectively.  $\epsilon_{Nd}$  values ( $-14.7$  to  $-15.4$ , av.  $-15.1$ ) and  $^{87}Sr/^{86}Sr$  ratios ( $0.7314$  to  $0.7318$ , av.  $0.7316$ ) of the sediments collected at the mouth of the Salween River were reported by Damodararao et al. (2016). Although isotope data of the river sediments in the western slopes of the IBA Ranges were unavailable, Nd and Sr isotope values of the Arakan shelf regions have been considered as an end-member of IBA Ranges (Colin et al., 1999; Miriyala et al., 2017), which is characterized by  $\epsilon_{Nd}$  values ( $-8.6$  to  $-8.9$ , av.  $-8.8$ ) and  $^{87}Sr/^{86}Sr$  ratios ( $0.7145$  to  $0.7148$ , av.  $0.7147$ ). Moreover, it was suggested that the Western Thailand is also a potential sediment provenance, despite a few data of the bed rock with  $\epsilon_{Nd}$  value (av.  $-25.2$ ) and  $^{87}Sr/^{86}Sr$  ratio (av.  $0.7764$ ) (Liew and McCulloch, 1985; Damodararao et al., 2016). As a local source, more radiogenic  $\epsilon_{Nd}$  values ( $> -4$  and  $5.2$ ) and less radiogenic  $^{87}Sr/^{86}Sr$  ratios ( $< 0.710$  and  $0.703$ ) were measured for both the Andaman Island and Barren Island (Lühr and Haldar, 2006; Awasthi et al., 2014).

## 3. Materials and methods

IODP Site U1447 ( $10^{\circ}47.40'N$ ,  $92^{\circ}59.99'E$ , with a water depth of  $1391$  m), has three drilled holes and is located  $\sim 45$  km offshore Little Andaman Island, within the Nicobar-Andaman Basin of the Andaman Sea (Fig. 1b). We used the sediment cores of Hole U1447A ( $\sim 738$  m in total depth). The sediments were classified into four distinct lithostratigraphic units (I to IV), which are composed of Holocene to late Miocene hemipelagic clays with a significant biogenic component, as well as a large number of thin calcitic turbidites (Clemens et al., 2016). Sampling was performed to select the hemipelagic sediments to avoid the turbidite layers as possible.

The age model at IODP Site U1447 was determined on the basis of nannofossil, planktonic foraminifera, and diatom datums with a few paleomagnetic reversal datums (Clemens et al., 2016). Biostratigraphic and magnetochron boundary datums align well at IODP Site U1447 (Fig. 2). Most biostratigraphic markers (calcareous nannofossil (*Discoaster hamatus*) and planktonic foraminifera (*Neoglobobulimina acostaensis*, *Globorotalia limbata*, *Thalassiosira burckliana*) dated the bottom of Hole U1447A to approximately  $9.43$  Ma the late Miocene (Fig. 2). Clemens et al. (2016) also reported that sedimentation rate was low (av.  $3.3$  cm/kyr) below  $700$  m CSF-A (the late Miocene), moderate (av.  $6.5$  cm/kyr) from  $700$  to  $\sim 300$  m CSF-A (Pliocene), and relatively high (av.  $12$  cm/kyr) above  $\sim 300$  m CSF-A (the Pleistocene).

**Table 1**  
Average  $\epsilon_{Nd}$  value and  $^{87}Sr/^{86}Sr$  ratio of potential end-members in the Andaman Sea.

End-member	Setting (core)	$\epsilon_{Nd}$	$^{87}Sr/^{86}Sr$	References
Irrawaddy River	Fluvial levee (I8)	$-7.3$	$0.7120$	Giosan et al. (2018)
	Beach ridge (I12)	$-6.9$	$0.7118$	Giosan et al. (2018)
	Beach ridge (I12)	$-6.8$	$0.7119$	Giosan et al. (2018)
Sittang River	Fluvial levee	$-10.4$	$0.7168$	Giosan et al. (2018)
Salween River	Mouth	$-14.7$	$0.7314$	Damodararao et al. (2016)
	Mouth	$-15.4$	$0.7318$	Damodararao et al. (2016)
IBA Ranges	Arakan shelf (MD77-178)	$-8.6$	$0.7145$	Colin et al. (1999)
	Arakan shelf (SK175/03)	$-8.9$	$0.7148$	Miriyala et al. (2017)
Western Thailand	Bed rock	$-23.0$	$0.7256$	Liew and McCulloch (1985)
	Bed rock	$-27.3$	$0.8272$	Liew and McCulloch (1985)
Andaman Island	Mithakhari Group	$> -4$	$< 0.710$	Awasthi et al. (2014)
Barren Island	Volcanics	$5.2$	$0.703$	Lühr and Haldar (2006)

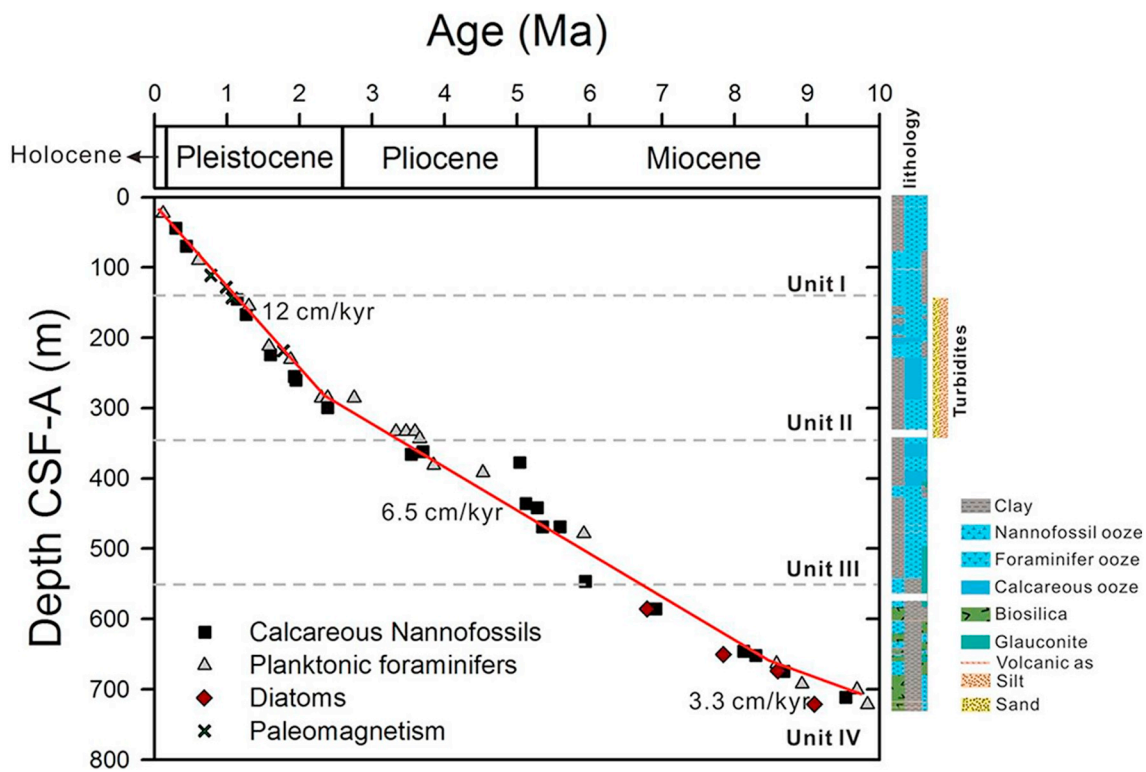


Fig. 2. The age model based on biostratigraphic and paleomagnetic data, sedimentation rate, and lithologic units (I, II, III, IV) with sediment compositions at IODP Site U1447 (Clemens et al., 2016).

Clay minerals (smectite, illite, kaolinite, and chlorite) were measured for 73 horizons using an X-ray diffractometer (Siemens/Bruker D5005) with CuK $\alpha$  Ni-filtered radiation at Gyeongsang National University. Prior to analysis, H<sub>2</sub>O<sub>2</sub> reagent was used to remove organic materials of the sediments. Fine-grained particles (< 2  $\mu$ m) were then separated by sedimentation based on Stokes' settling velocity law. Air-dried and ethylene-glycolated oriented mounts were prepared using "the smear-on-glass slide" method (Stokke and Carson, 1973). Clay minerals were identified using basal reflections and the classifications of Moore and Reynolds (1989). Semi-quantitative estimates (weighted peak area %) of the clay minerals were calculated using the Biscaye (1965) procedure.

Nd and Sr isotope analyses were performed on 17 sediment samples (12 samples of clay-sized (< 2  $\mu$ m) particles and 5 samples of bulk sediments) using the thermal ionization mass spectrometry at the Korea Basic Science Institute: First, carbonate, Fe-Mn oxide, and biogenic silica components were removed using 1.5 M acetic acid, 0.05 M Hydroxylamine hydrochloride, and 1 M NaOH, respectively. Subsequently, about 0.1 g of each sediment sample was dissolved using a mixture of concentrated HF, HNO<sub>3</sub>, and HClO<sub>4</sub>, and the subsequent separation of Nd and Sr from the final residue followed procedures by Pin and Zalduegui (1997). Sr and Nd isotope ratios were normalized to <sup>86</sup>Sr/<sup>88</sup>Sr = 0.1194 and <sup>146</sup>Nd/<sup>144</sup>Nd = 0.7219, respectively. Analysis of the Sr standard NBS 987 and the Nd standard JNdi-1 (Tanaka et al., 2000) resulted in <sup>87</sup>Sr/<sup>86</sup>Sr = 0.710245  $\pm$  4 (2SD, n = 4) and <sup>143</sup>Nd/<sup>144</sup>Nd = 0.512097  $\pm$  5 (2SD, n = 4). The  $\epsilon_{Nd}$  parameter was calculated using a <sup>143</sup>Nd/<sup>144</sup>Nd value of 0.512638 for the CHUR (Chondritic Uniform Reservoir: Hamilton et al. (1983)), as follows.

$$\epsilon_{Nd} = \left[ \frac{\left( \frac{^{143}\text{Nd}}{^{144}\text{Nd}} \right)_{\text{sample}}}{0.512638} - 1 \right] \times 10,000 \quad (1)$$

We measured  $\delta^{13}\text{C}_{\text{SOM}}$  values for 41 sediment samples using elemental analysis-isotope ratio mass spectrometry (EA-IRMS: Europa Scientific 20-20 mass spectrometer) at Iso-Analytical Ltd. (UK). Each 100 mg sample was treated to remove CaCO<sub>3</sub> using 10% HCl before analysis. Isotope values were expressed in conventional delta notation relative to the Vienna Pee Dee Belemnite (V-PDB). The reference material used during  $\delta^{13}\text{C}$  analysis was IA-R001 (wheat flour,  $\delta^{13}\text{C}_{\text{V-PDB}} = -26.43\text{‰}$ ). For quality control purposes check samples of IA-R001, IA-R005 (beet sugar,  $\delta^{13}\text{C}_{\text{V-PDB}} = -26.03\text{‰}$ ) and IA-R006 (cane sugar,  $\delta^{13}\text{C}_{\text{V-PDB}} = -11.64\text{‰}$ ) were also analyzed. IA-R001, IA-R005 and IA-R006 are calibrated against and traceable to IAEA-CH-6 (sucrose,  $\delta^{13}\text{C}_{\text{V-PDB}} = -10.43\text{‰}$ ). IAEA-CH-6 is an inter-laboratory comparison standard distributed by the International Atomic Energy Agency, Vienna. Precision for  $\delta^{13}\text{C}_{\text{SOM}}$  was approximately  $\pm 0.08\text{‰}$ .

#### 4. Results

Clay mineral compositions (smectite, illite, kaolinite, and chlorite) at IODP Site 1447 consist mainly of smectite (17 to 65%) and illite (19 to 47%), with smaller amounts of chlorite (5 to 17%) and kaolinite (9 to 20%) (Fig. 3a–d). Despite different time-scale, core MD77-169 in the Andaman Sea shows a consistent range of clay mineral composition over the last 280 ka (Colin et al., 1999). Our results are also very similar to the clay mineralogy measured in Pleistocene and late Miocene sediments from NGHP Site 17 (Phillips et al., 2014). The variation patterns of illite, chlorite, and kaolinite contents are opposite to that smectite (Fig. 3a–d). Downcore variation of clay mineral composition shows that smectite content decreased gradually from the late Miocene (58–51%) to the late Pleistocene-Holocene (30–20%) with distinct decrease at  $\sim 9.2$  to 8.5 Ma,  $\sim 3.6$  Ma,  $\sim 2.4$  Ma, and  $\sim 1.2$  Ma (Fig. 3a–d). In addition, the distinct peaks of these minerals occur synchronously with marked decrease of smectite content.

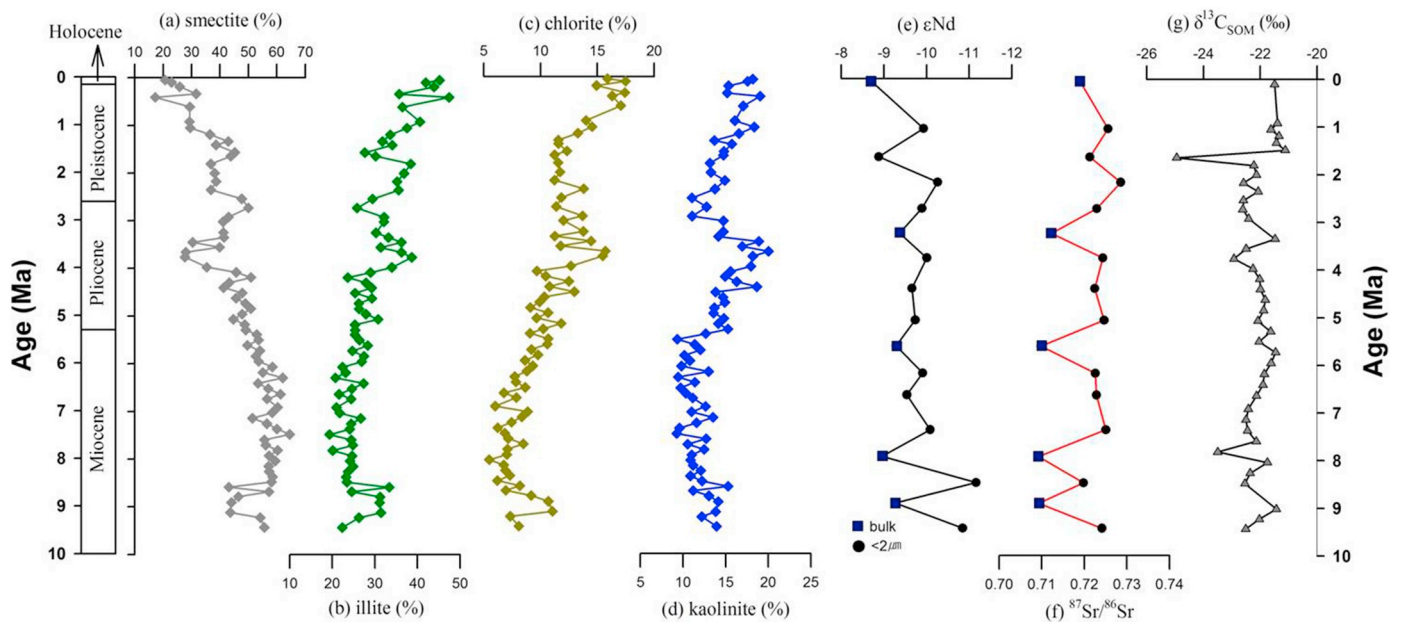


Fig. 3. Downcore variations in (a) smectite content, (b) illite content, (c) kaolinite content, (d) chlorite content, (e)  $\epsilon_{Nd}$  values, (f)  $^{87}Sr/^{86}Sr$  ratios, and (g)  $\delta^{13}C_{SOM}$  values at IODP Site U1447 during the last 10 Ma.

The downcore profiles of Nd and Sr isotope values at IODP Site U1447 show that  $\epsilon_{Nd}$  values have varied within range from  $-11.2$  to  $-8.7$  (av.  $-9.7$ ) and  $^{87}Sr/^{86}Sr$  ratios have changed between  $0.709$  and  $0.729$  (av.  $0.720$ ) since the late Miocene (Fig. 3e and f). These isotope values are similar to the previous results ( $-11.5$  to  $-8.8$  for  $\epsilon_{Nd}$  values and  $0.712$  to  $0.722$  for  $^{87}Sr/^{86}Sr$  ratios) of the Holocene and Last Glacial Maximum (LGM) sediments in the Andaman Sea cores RC12-344, MD77-171, and MD77-169 (Colin et al., 1999). In this study,  $\epsilon_{Nd}$  value (av.  $-10.0$ ) of the fine-grained sediments is almost similar to that (av.  $-9.1$ ) of bulk sediments (Fig. 3e). In contrast,  $^{87}Sr/^{86}Sr$  ratios between the fine-grained (av.  $0.724$ ) and bulk (av.  $0.712$ ) sediments are distinctly different, showing that  $^{87}Sr/^{86}Sr$  ratios of the fine-grained sediments are notably higher than those of bulk sediments (Fig. 3f). Despite the different  $^{87}Sr/^{86}Sr$  ratios between bulk and the fine-grained sediments, overall variations of  $\epsilon_{Nd}$  values and  $^{87}Sr/^{86}Sr$  ratios at IODP Site U1447 have been low since the late Miocene.

$\delta^{13}C_{SOM}$  values at IODP Site U1447 varied within the limited range from  $-21.1\text{‰}$  to  $-23.5\text{‰}$ , except for a sample (220 CSF-A m) of  $-24.9\text{‰}$  belonging to a thick turbidite at  $\sim 1.6$  Ma (Fig. 3g). Our results at IODP Site U1447 are similar to the  $\delta^{13}C_{SOM}$  values (between  $-20.2\text{‰}$  and  $-23.0\text{‰}$ ) measured at NGHP Site 17 (13 km to the southeast in the Andaman accretionary wedge) in Pleistocene and late Miocene sediments (Johnson et al., 2014). The average  $\delta^{13}C_{SOM}$  values before  $1.5$  Ma was  $-22.2\text{‰}$  and it increased up  $-21.4\text{‰}$  after that. It is of note that higher  $\delta^{13}C_{SOM}$  values after  $1.5$  Ma and  $\sim 3.5$  Ma correspond to low S/(I + C) ratios.

## 5. Discussion

### 5.1. Sediment provenance change in the Andaman Sea since the late Miocene

The long-term variations of clay minerals at IODP Site U1447 are clearly characteristic (Fig. 3a–d); gradual decreasing smectite content and increasing illite, kaolinite, and chlorite content from the late Miocene to the Pleistocene. A similar variation pattern of clay minerals from the late Miocene and the Pleistocene were already reported from core NGHP 17 collected near IODP Site U1447 (Phillips et al., 2014). Such kind variations of clay minerals are controlled by either sediment provenance (e.g., Liu et al., 2012; Wan et al., 2012) or weathering

patterns in response to climatic changes (e.g., Colin et al., 1999; Liu et al., 2004). For example, Wan et al. (2012) interpreted that higher illite/smectite values in the West Philippine Sea during glacial periods are attributed to sediment provenance change of more eolian input from central Asia and less smectite from volcanic rocks on Luzon Island. In contrast, Liu et al. (2004) suggested that the ratio of smectite to the sum of illite and chlorite (i.e., S/(I + C)) during the last 190 kyr in the South China Sea has been controlled by monsoon-controlled chemical weathering versus physical erosion over the eastern Tibetan Plateau and the Mekong Basin. Thus, the variation of clay mineral compositions at IODP Site U1447 during the last 10 Ma can be attributable to either sediment provenance or weathering activity.

Nd isotopic ratios of silicate particles are almost not altered during the processes of weathering, transport, and sedimentation, and can be a powerful tool to trace provenance of the terrigenous fraction of marine sediments (Blum and Erel, 2003).  $\epsilon_{Nd}$  values (av.  $-9.1$ ) of bulks sediments are similar to those (av.  $-10.0$ ) of fine-grained sediments at IODP Site U1447 (Fig. 3e). However,  $^{87}Sr/^{86}Sr$  ratios (av.  $0.712$ ) of bulk sediments are lower than those (av.  $0.724$ ) of fine-grained particles (Fig. 3f).  $^{87}Sr/^{86}Sr$  isotopic ratios are more susceptible to the influence of weathering related to grain size fractions (Blum and Erel, 2003). Our results also confirm grain size effect on Sr isotopic ratios, resulting in higher  $^{87}Sr/^{86}Sr$  ratios for finer-grained particles. Despite grain size effect, Sr isotope compositions of detrital fine fraction in marine sediments at IODP Site U1447 have remained consistent since the late Miocene, similarly to  $\epsilon_{Nd}$  values (Fig. 3e and f). This indicates that sediment provenance has not changed significantly since the late Miocene, although our low-resolution measurement cannot detect high-resolution (orbital-scale) changes. It also proves that the clay mineral compositions have not been affected by the sediment provenance change.

Based on the previously published data of six potential source regions (Table 1), we plotted  $\epsilon_{Nd}$  values and  $^{87}Sr/^{86}Sr$  ratios of our results to determine the sediment source to IODP Site U1447 in the western Andaman Sea (Fig. 4).  $\epsilon_{Nd}$  values and  $^{87}Sr/^{86}Sr$  ratios at IODP U1447 vary from  $-11.2$  to  $-8.7$  (av.  $-9.7$ ) and  $0.709$  and  $0.729$  (av.  $0.720$ ), respectively. Despite a slight discrepancy of  $^{87}Sr/^{86}Sr$  ratios between bulk and fine-grained sediments, Nd and Sr isotope values at IODP Site U1447 were placed within a range of four end-members: Irrawaddy River, Salween River, Sittang River, and the IBA Ranges being distinctly

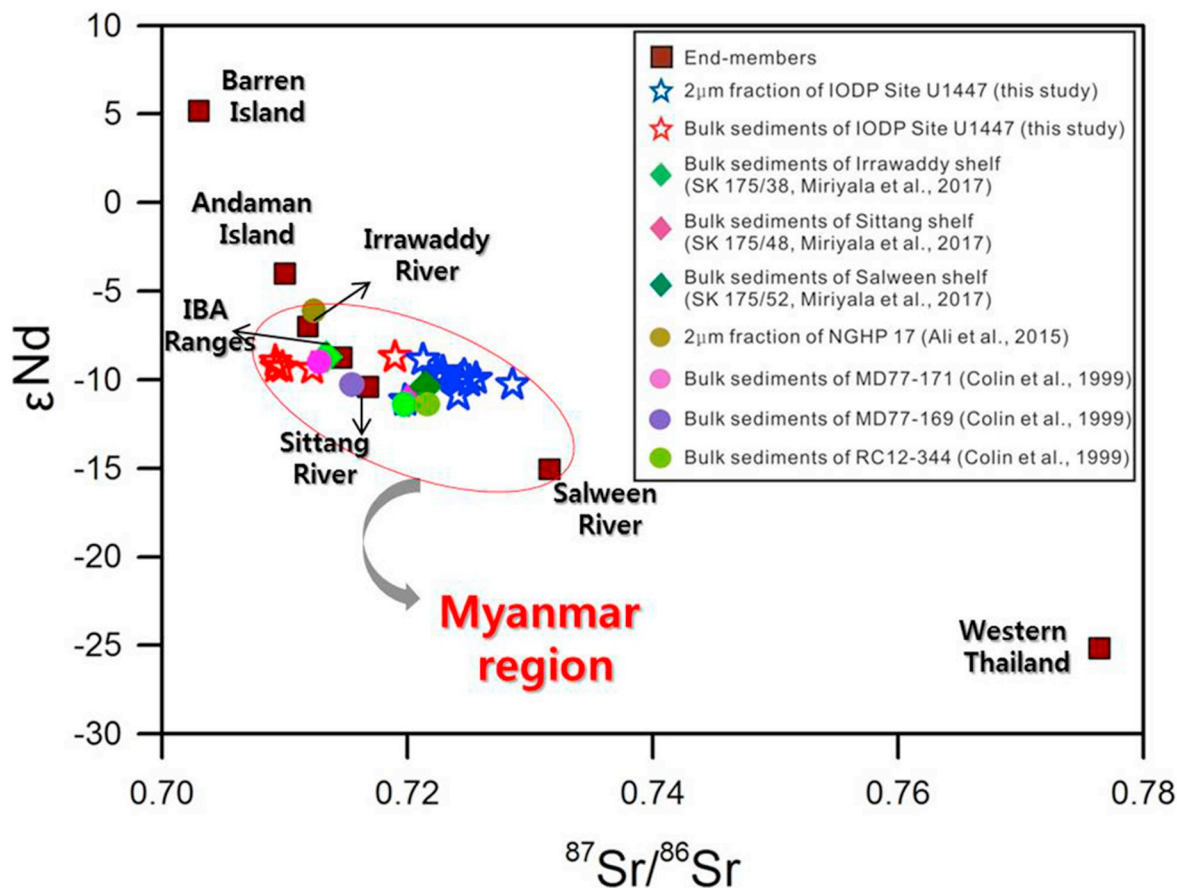


**Fig. 4.** Biplot of  $\epsilon_{Nd}$  values and  $^{87}Sr/^{86}Sr$  isotopic ratios at IODP Site U1447, showing the prominent sediment provenances. Six potential end-member values (Indo-Burma-Arakan (IBA) Ranges ( $\epsilon_{Nd}$ :  $-8.8$ ,  $^{87}Sr/^{86}Sr$  ratios:  $0.715$ ), Irrawaddy River ( $\epsilon_{Nd}$ :  $-7.0$ ,  $^{87}Sr/^{86}Sr$  ratios:  $0.712$ ), Salween River ( $\epsilon_{Nd}$ :  $-15.1$ ,  $^{87}Sr/^{86}Sr$  ratios:  $0.732$ ), Sittang River ( $\epsilon_{Nd}$ :  $-10.4$ ,  $^{87}Sr/^{86}Sr$  ratios:  $0.717$ ), Tanintharyi River ( $\epsilon_{Nd}$ :  $-25.2$ ,  $^{87}Sr/^{86}Sr$  ratios:  $0.776$ ), and Andaman Island ( $\epsilon_{Nd}$ :  $> -4$ ,  $^{87}Sr/^{86}Sr$  ratios:  $< 0.710$ ), and Barren Island ( $\epsilon_{Nd}$ :  $5.2$ ,  $^{87}Sr/^{86}Sr$  ratios:  $0.703$ )) were taken from the previous studies (Colin et al., 1999; Luhr and Haldar, 2006; Awasthi et al., 2014; Damodararao et al., 2016; Miriyala et al., 2017; Giosan et al., 2018).

differentiated from Western Thailand, the volcanic islands (Andaman Island, and Barren Island) (Fig. 4). Our results are similar to those of the shelf sediments off the mouth of Irrawaddy River ( $\epsilon_{Nd}$ :  $-8.7$  and  $^{87}Sr/^{86}Sr$ :  $0.713$  from core SK175/38), Salween River ( $\epsilon_{Nd}$ :  $-10.4$  and  $^{87}Sr/^{86}Sr$ :  $0.722$  from core SK175/52), and Sittang River ( $\epsilon_{Nd}$ :  $-11.2$  and  $^{87}Sr/^{86}Sr$ :  $0.720$  from core SK175/48) in the Andaman Sea (Miriya et al., 2017). Moreover, our results also similar to those of core sediments ( $\epsilon_{Nd}$ :  $-11.4$  and  $^{87}Sr/^{86}Sr$ :  $0.720$  for RC12-344,  $\epsilon_{Nd}$ :  $-9.0$  and  $^{87}Sr/^{86}Sr$ :  $0.713$  for MD77-171, and  $\epsilon_{Nd}$ :  $-10.6$  and  $^{87}Sr/^{86}Sr$ :  $0.716$  for MD77-169) in the Andaman Sea (Colin et al., 1999). Because of the strong clockwise surface flow during the Indian summer monsoon, sediment from Western Thailand may be prevented being transported to the western Andaman Sea. In addition, although the summer monsoon surface current transports sediments derived from the Ganges-Brahmaputra River system ( $\epsilon_{Nd}$ :  $-16.1$  and  $^{87}Sr/^{86}Sr$ :  $0.746$ ) into the Andaman Sea (Robinson et al., 2007), our results indicate that the amount of these sediments deposited at IODP Site U1447 may be insignificant, compared with those from the Myanmar region.

It should be of note that the isotope data at IODP Site U1447 are somewhat different from those (av.  $\epsilon_{Nd}$ :  $-6.1$  and av.  $^{87}Sr/^{86}Sr$ :  $0.712$ ) of core NGHP 17 in the western Andaman Sea, although Nd and Sr isotopes were measured for clay-sized fraction of core NGHP 17 by ICP-MS (Ali et al., 2015). Ali et al. (2015) reported that the sediments of core NGHP 17 were transported mainly from the Irrawaddy River similar to our results, but suggested additional small contribution from more radiogenic Nd isotope source such as Barren Island during the past 60 ka. At the tectonic time-scale during the last 10 Ma, the contribution

of volcanic materials to the study area is difficult to estimate. Despite being speculative, a slight discrepancy of isotope signatures between IODP Site U1447 and NGHP 17 may be due to more recent volcanic activity in the western Andaman Sea. Nonetheless, the sediments at IODP Site U1447 consist of a mixture mostly sourced from the Irrawaddy River, the Salween River, the Sittang River, and the IBA Ranges (i.e., Myanmar region) since the late Miocene, and we concluded that sediment provenances at IODP Site U1447 has not been changed dramatically during the last 10 Ma.

## 5.2. Paleoclimate change and weathering activity by Indian monsoon in the Myanmar region

Because of no significant change of sediment provenance based on Nd/Sr isotope systematics, the long-term variation of clay mineral compositions during the last 10 Ma has been attributed to the other factors. The distribution of clay minerals in the deep sea marine sediments can be attributed to sea level changes in addition to provenance shifts (Steinke et al., 2008). During the low sea level condition, the river mouth changes may result in the different contribution of clay minerals to the deep sea environment. In addition, more sediments were transported toward the deep sea environment through active slope failure or frequent turbidity currents. However, such kind of different depositional processes may not be a significant factor to influence the clay mineral compositions in the study area. Thus, the long-term variation of clay mineral compositions at IODP Site U1447 should be related to the weathering activity, not to the sediment provenance or depositional

processes related to sea level change.

Illite and chlorite are considered primary clay minerals mainly produced by physical erosion of igneous and metamorphic rocks under cold and dry climatic conditions (Allen et al., 2008), whereas smectites are considered secondary clay minerals formed under warm and humid climatic conditions by intense chemical weathering (Chamley, 1989). Consequently, more illite and chlorite are expected under dominant physical weathering condition during Indian winter monsoon whereas more smectite are expected under dominant chemical weathering condition during Indian summer monsoon. Thus, S/(I + C) ratio at IODP Site U1447 serves as a proxy to estimate the variation of weathering patterns in the Myanmar region in response to Indian summer/winter monsoon intensity. High S/(I + C) ratios represent strong chemical weathering and/or weak physical weathering under warm and humid climate with heavy precipitation (i.e., a strong Indian summer monsoon/weak Indian winter monsoon), whereas low ratios indicate weak chemical weathering or strong physical weathering under cold and dry climate with low precipitation (i.e., a weak Indian summer monsoon/strong Indian winter monsoon). Colin et al. (2006) reported variation of S/(I + C) ratio in the Andaman Sea during the 200 ka was closely related to Indian monsoon strength controlling an amount of precipitation and rainfall.

Fig. 5 compiles the different proxy data of long-term global climate change to support our results during the last 10 Ma. The long-term variation of S/(I + C) ratios at IODP Site U1447 is characterized by gradual decreasing trend since ~10 Ma, which coincides with the long-term global climate cooling represented by  $\delta^{18}\text{O}$  values (Fig. 5a and b). This coincidence simply indicates that physical weathering (chemical weathering) in the Myanmar region became stronger (weaker) with less precipitation since the late Miocene. Thus, the temporal weathering pattern changes in the Myanmar region based on clay mineral composition changes at IODP Site U1447 suggest that Indian winter (summer) monsoon became intensified (weakened) since the late Miocene. Such gradual change of Indian monsoon strength was substantiated by other records: 1) based on  $\delta^{13}\text{C}$  values of leaf waxes,  $\text{C}_4$  plant expansion recorded at ODP Site 722 in the Arabian Sea reflected

an increase of dryness in the Arabian Peninsula (Huang et al., 2007; Fig. 5c), 2) decreasing CIA at Indus Marine A1 in the Arabian Sea showed the gradual strengthening of dryness condition (Clift et al., 2008; Fig. 5d), and 3) the variations of clay mineral compositions at IODP Site U1456 in the Arabian Sea (Chen et al., 2018) and in the Zhaotong Basin on the southeastern margin of the Tibetan Plateau (Li et al., 2019) reflected increasing physical weathering under the dominant dry condition (Fig. 5e and f). All these records substantiate that Indian winter monsoon increased gradually stronger in coincidence with global cooling trends. Furthermore, the East Asian monsoon system also corroborated similar long-term variation patterns: 1) decreasing Rb/Sr ratios at IODP Site 1146 in the South China Sea reflected the reduced chemical weathering (Wan et al., 2010; Fig. 5g), 2) increasing abundance of black carbons at IODP Site 1148 in the South China Sea showed an increase of dryness (Jia et al., 2003; Fig. 5h), and 3) increasing illite/smectite (I/S) ratios at IODP Site 1430 in the East Sea (Japan Sea) resulted from enhanced dryness in the Central Asia (Shen et al., 2017; Fig. 5i), all of which were controlled by the weak intensity of East Asian summer monsoon (or strong intensity of East Asian winter monsoon) since the late Miocene. Thus, the strengthening (or weakening) of physical (or chemical) weathering patterns are closely related to the monsoon intensity change in association with global climate cooling.

The gradual decrease of S/(I + C) ratios at IODP Site U1447 during the last 10 Ma was accompanied by four distinct drops at ~9.2–8.5 Ma, ~3.6 Ma, ~2.4 Ma, and ~1.2 Ma (Fig. 6b). Because the global cooling by  $\delta^{18}\text{O}$  values did not occur at these times (Fig. 6a), additional mechanism must have been considered. An et al. (2001) reported, based on modulating the atmospheric circulation and its barrier effect to sourced moisture, that uplift of the Tibetan Plateau played an important role in changing the Asian monsoon intensity and Asian aridity. The aridity in the central Myanmar region has been usually attributed to the rain shadow effect of the Indo-Burman Ranges, interrupting moisture supply by the Indian summer monsoon (Zin-Maung-Maung-Thein et al., 2011; Damodarao et al., 2016). Zin-Maung-Maung-Thein et al. (2011) also reported that the aridity conditions have been likely controlled by the

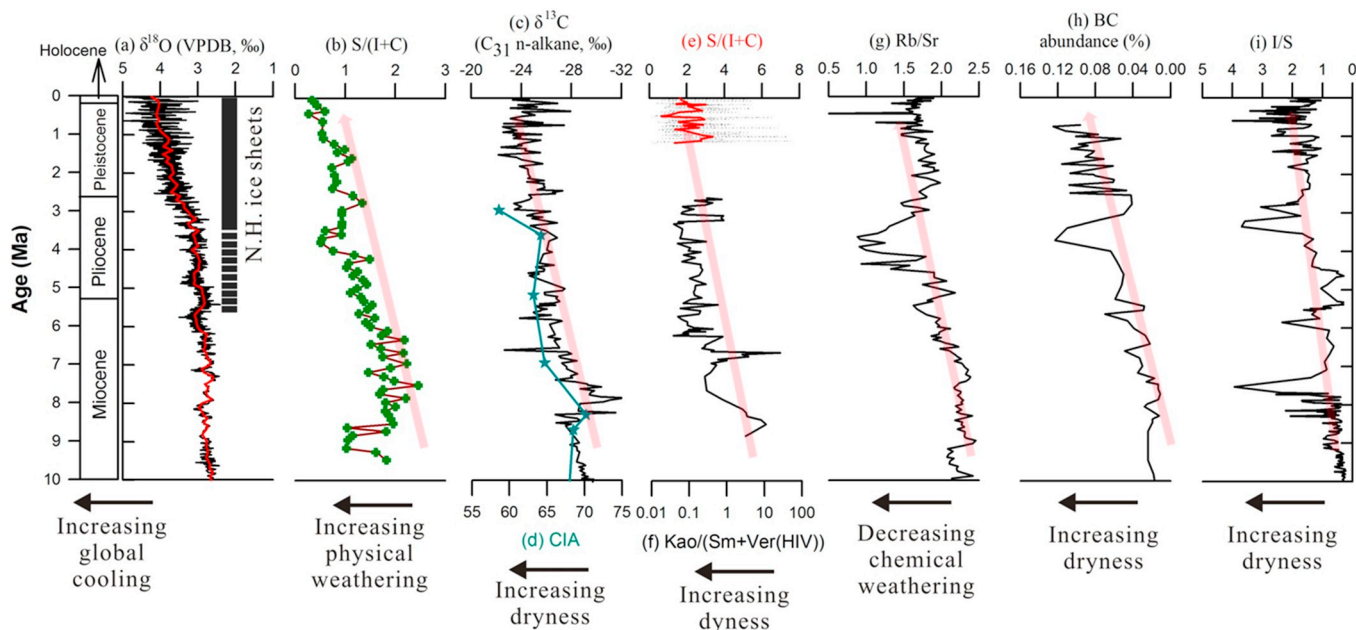


Fig. 5. Long-term evolution of global climate change and Indian and East Asian monsoons over the last 10 Ma. (a) global  $\delta^{18}\text{O}$  data of deep-sea benthic foraminifera (Zachos et al., 2001), (b) S/(I + C) ratios at IODP Site U1447 in the Andaman Sea (this study), (c)  $\delta^{13}\text{C}$  ( $\text{C}_{31}$  n-alkane) values at ODP Site 722 in the Arabian Sea (Huang et al., 2007), (d) CIA values at Indus Marine A1 in the Arabian Sea (Clift et al., 2008), (e) S/(I + C) ratios at IODP Site U1456 in the Arabian Sea (Chen et al., 2018), (f) kaolinite/(smectite + vermiculite) [Kao/(Sm + Ver(HIV))] ratios at the Zhaotong Basin on the southeastern margin of the Tibetan Plateau (Li et al., 2019), (g) Rb/Sr ratios at IODP Site 1146 in the South China Sea (Wan et al., 2010), (h) Black carbon (BC) abundance at IODP Site 1148 in the South China Sea (Jia et al., 2003), (i) I/S ratios at IODP Site U1430 in the East Sea (Sea of Japan) (Shen et al., 2017).

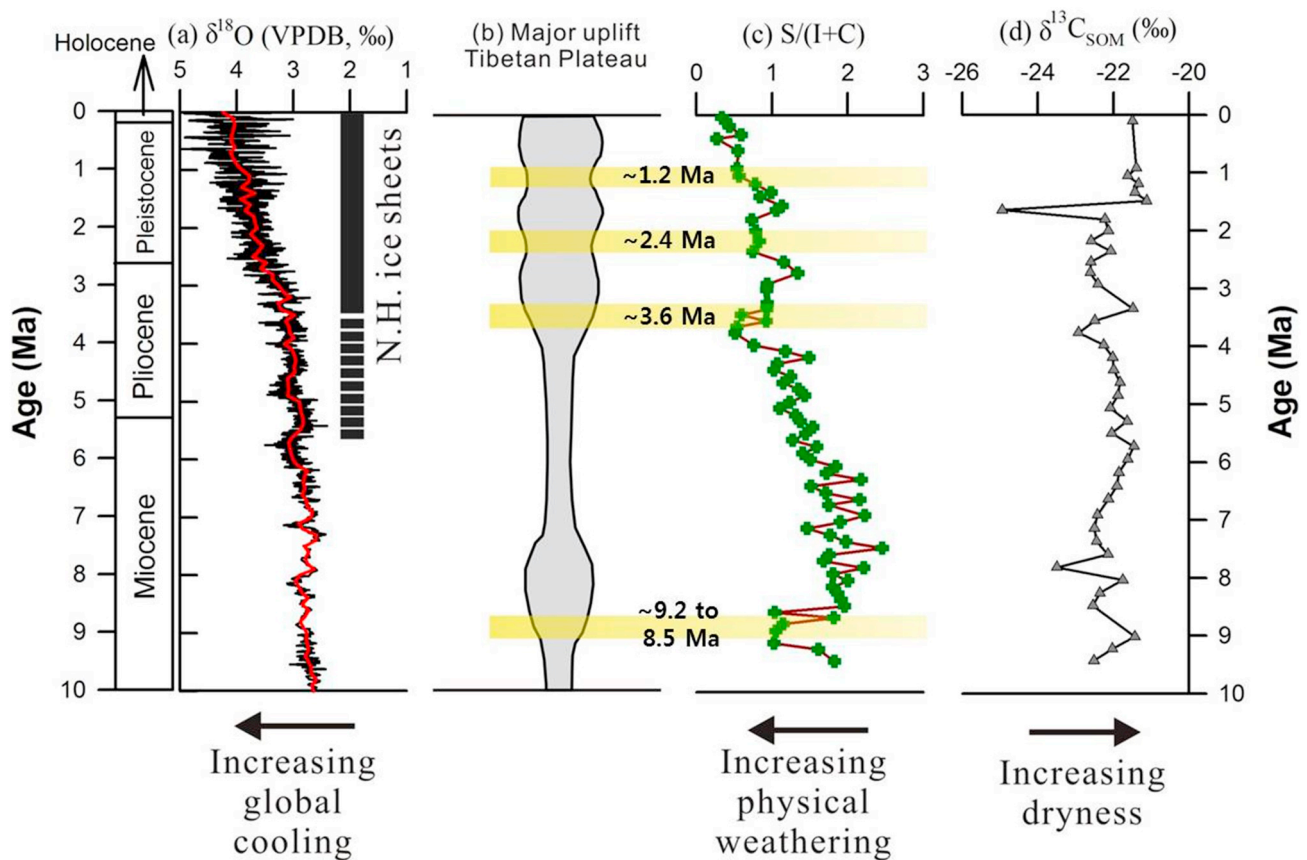


Fig. 6. Comparison of (a) global  $\delta^{18}\text{O}$  data of deep-sea benthic foraminifera (Zachos et al., 2001), (b) the major uplift of Tibetan Plateau (TP) (Li et al., 2014), (c) distinct decrease of S/(I + C) ratios, (d)  $\delta^{13}\text{C}_{\text{SOM}}$  values at IODP Site U1447.

uplift of the Indo-Burman Ranges as a result of the Himalaya-Tibetan Plateau Orogeny during the late Neogene. The Indo-Burman Ranges are located in the southern branch of the Himalayan-Tibetan Plateau, which experienced a series of significant uplift (i.e., the rapid rise at  $\sim 8$  Ma,  $\sim 3.6$  Ma,  $\sim 2.6$  Ma, 1.8–1.7 Ma, 1.2–0.6 Ma and 0.15 Ma) since the late Miocene (Li et al., 2014). These timings of rapid rising of Tibetan Plateau coincide with four times of markedly declining S/(I + C) ratios at IODP Site U1447 (Fig. 6c). Thus, our results suggest that the distinct decrease of S/(I + C) ratios, indicating more strengthening physical weathering (or more weakening chemical weathering), are attributed to a combined effect of the uplift of Tibetan Plateau and global cooling.

The aridity is an important factor to distribute the vegetation in the continental regions (Jia et al., 2003; Huang et al., 2007). Huang et al. (2007) reported, based on  $\delta^{13}\text{C}$  values of plant leaf waxes at ODP Site 722 in the Arabian Sea, that the increased aridity triggered the expansion of  $\text{C}_4$  plants in the Arabian Peninsula and Himalayan foreland since the late Miocene. Jia et al. (2003) also proposed that expansion of  $\text{C}_4$  plants in the East Asia has been affected by the increased aridity due to monsoon climate change. Thus,  $\delta^{13}\text{C}_{\text{SOM}}$  values at IODP Site U1447 may reflect vegetation changes in the Myanmar region.  $\delta^{13}\text{C}_{\text{SOM}}$  values at IODP Site U1447 were higher after 1.5 Ma and  $\sim 3.5$  Ma when S/(I + C) ratios were minima (Fig. 6d). It seems to indicate that  $\text{C}_4$  plant increased under dominant physical weathering environment in the Myanmar region.  $\delta^{13}\text{C}_{\text{SOM}}$  values at NGHP Site 17 increased from  $-22\text{‰}$  to  $-20\text{‰}$  during the Pleistocene with increasing C/N ratios (Johnson et al., 2014). It is also consistent with our records, supporting the gradual vegetation shift of  $\text{C}_4$  plant, despite requirement of further analyses.

## 6. Conclusions

In this study, we revealed sediment provenance changes based on detrital Nd-Sr isotopes and discussed the long-term evolution of the Indian monsoon based on clay mineral compositions of fine-grained sediments at IODP Site U1447 in the western Andaman Sea. The detrital Nd-Sr isotope systematics substantiates that the sediment source to IODP Site U1447 remained unchanged since the late Miocene and that terrigenous particles have primarily originated from the Myanmar region (the Irrawaddy River, Salween River, Sittang River, and IBA Ranges). As a result, the variations of clay minerals at IODP Site U1447 are controlled primarily by the climate changes, not by sediment provenance shifts related to the sea level change and depositional processes. Thus, S/(I + C) ratios of clay mineral compositions can be used as a proxy to reconstruct weathering intensity (i.e., climate change) in terms of Indian monsoon evolution. The steady increase of S/(I + C) ratios at IODP Site U1447 indicates that the physical weathering in the Myanmar region intensified gradually since the late Miocene, reflecting consistent increasing dryness in the source region due to strong Indian winter monsoon (or weak Indian summer monsoon). These long-term variations of Indian monsoon seem to be closely related with the global climate cooling. In addition, drastic dryness at  $\sim 9.2$ – $8.5$  Ma,  $\sim 3.6$  Ma,  $\sim 2.4$  Ma, and  $\sim 1.2$  Ma has been affected by a combination of the global climate cooling and the uplift of Tibetan Plateau as a local effect.  $\delta^{13}\text{C}_{\text{SOM}}$  values at IODP Site U1447 were higher after 1.5 Ma and  $\sim 3.5$  Ma when S/(I + C) ratios were minima, which may indicate that  $\text{C}_4$  plant increased under dominant physical weathering environment in the Myanmar region resulting from the strong Indian winter monsoon (or weak Indian summer monsoon).

## Acknowledgements

We would like to thank the co-chiefs, staff scientist, and shipboard scientists of IODP Expedition 353, as well as the captain and crew of the *D/V JOIDES Resolution*. We also thank participants in the core sampling party and the staff of the Kochi Core Center for their assistance. Constructive comments by editor and three anonymous reviewers for the improvement of data interpretation were greatly appreciated. This research was supported by the National Research Foundation of Korea (2016R1A2B4008256 and 2019R1A2C1007701; to BKK) and partly by K-IODP program (to SK) and KOPRI project (PE19030; to JIL).

## Appendix A. Supplementary data

Supplementary data to this article can be found online at <https://doi.org/10.1016/j.palaeo.2019.109339>.

## References

- Ali, S., Hathorne, E.C., Frank, M., Gebregiorgis, D., Statterger, K., Stumpf, R., Kutterolf, S., Johnson, J.E., Giosan, L., 2015. South Asian monsoon history over the past 60 kyr recorded by radiogenic isotopes and clay mineral assemblages in the Andaman Sea. *Geochemistry, Geophysics, Geosystems* 16, 505–521. <https://doi.org/10.1002/2014GC005586>.
- Allen, R., Najman, Y., Carter, A., Barfod, D., Bickle, M., Chapman, H., Garzanti, E., Vezzoli, G., Ando, S., Parrish, R.R., 2008. Provenance of the Tertiary sedimentary rocks of the Indo-Burman Ranges, Burma (Myanmar): Burman arc or Himalayan-derived? *Journal of the Geological Society* 165, 1045–1057. <https://doi.org/10.1144/0016-76492007-143>.
- An, Z., Kutzbach, J.E., Prell, W.L., Porter, S.C., 2001. Evolution of Asian monsoons and phased uplift of the Himalaya–Tibetan plateau since Late Miocene times. *Nature* 411, 62–66. <https://doi.org/10.1038/35075035>.
- Awasthi, N., Ray, J. S., Singh, A. K., Band, S. T., and Rai, V. K., 2014. Provenance of the Late Quaternary sediments in the Andaman Sea: implications for monsoon variability and ocean circulation. *Geochemistry, Geophysics, Geosystems*, 15, 3890–3906. <https://doi.org/10.1002/2014GC005462>.
- Biscaye, P.E., 1965. Mineralogy and sedimentation of recent deep-sea clay in the Atlantic Ocean and adjacent seas and oceans. *Geological Society of America Bulletin* 76, 803–832. [https://doi.org/10.1130/0016-7606\(1965\)76\[803:MASORD\]2.0.CO;2](https://doi.org/10.1130/0016-7606(1965)76[803:MASORD]2.0.CO;2).
- Blum, J., Erel, Y., 2003. Radiogenic isotopes in weathering and hydrology. *Treatise on Geochemistry* 5, 605. [https://doi.org/10.1130/00167606\(1965\)76\[803:MASORD\]2.0.CO;2](https://doi.org/10.1130/00167606(1965)76[803:MASORD]2.0.CO;2).
- Cawthorn, T., Johnson, J., Giosan, L., Flores, J., Rose, K., Solomon, E., 2014. A late Miocene–early Pliocene biogenic silica crash in the Andaman Sea and Bay of Bengal. *Marine and Petroleum Geology* 58, 490–501. <https://doi.org/10.1016/j.marpetgeo.2014.07.026>.
- Chamley, H., 1989. *Clay Sedimentology*. Berlin, Germany, Springer-Verlag, 267pp. [doi.org/10.1007/978-3-642-85916-8-2](https://doi.org/10.1007/978-3-642-85916-8-2).
- Chen, H., Xu, Z., Clift, P. D., Lim, D., Khim, B.-K., and Yu, Z., 2018. Orbital-scale evolution of the Indian summer monsoon since 1.2 Ma: evidence from clay mineral records at IODP Expedition 355 Site U1456 in the eastern Arabian Sea. *Journal of Asian Earth Sciences* 174, 11–22. [doi.org/10.1016/j.jseaes.2018.10.012](https://doi.org/10.1016/j.jseaes.2018.10.012).
- Clemens, S.C., Kuhnt, W., LeVay, L.J., and the Expedition 353 Scientists, 2016. Indian monsoon rainfall. *Proceedings of the International Ocean Discovery Program*, 353: College Station, TX (International Ocean Discovery Program). [10.14379/iodp.proc.353.107.2016](https://doi.org/10.14379/iodp.proc.353.107.2016).
- Clift, P.D., Hodges, K.V., Heslop, D., Hannigan, R., Van Long, H., Calves, G., 2008. Correlation of Himalayan exhumation rates and Asian monsoon intensity. *Nature Geoscience* 1, 875–880. <https://doi.org/10.1038/ngeo351>.
- Colin, C., Turpin, L., Bertaux, J., Desprairies, A., Kissel, C., 1999. Erosional history of the Himalayan and Burman ranges during the last two glacial–interglacial cycles. *Earth and Planetary Science Letters* 171, 647–660. [doi.org/10.1016/S0012-821X\(99\)00184-3](https://doi.org/10.1016/S0012-821X(99)00184-3).
- Colin, C., Turpin, L., Blamart, D., Frank, N., Kissel, C., Duchamp, S., 2006. Evolution of weathering patterns in the Indo-Burman Ranges over the last 280 kyr: effects of sediment provenance on  $^{87}\text{Sr}/^{86}\text{Sr}$  ratios tracer. *Geochemistry, Geophysics, Geosystems* 7. <https://doi.org/10.1029/2005GC000962>.
- Curray, J.R., 2005. Tectonics and history of the Andaman Sea region. *Journal of Asian Earth Sciences* 25, 187–232. [doi.org/10.1016/J.JSEAES.2004.09.001](https://doi.org/10.1016/J.JSEAES.2004.09.001).
- Damodararao, K., Singh, S.K., Rai, V.K., Ramaswamy, V., Rao, P., 2016. Lithology, monsoon and sea-surface current control on provenance, dispersal and deposition of sediments over the Andaman continental shelf. *Frontiers in Marine Science* 3, 118. [doi.org/10.3389/fmars.2016.00118](https://doi.org/10.3389/fmars.2016.00118).
- Derry, L., France-Lanord, C., 1996. Neogene Himalayan weathering history and river  $^{87}\text{Sr}/^{86}\text{Sr}$ : impact on the marine Sr record. *Earth and Planetary Science Letters* 142, 59–74. [doi.org/10.1016/0012-821X\(96\)00091-X](https://doi.org/10.1016/0012-821X(96)00091-X).
- Flores, J.A., Johnson, J.E., Mejía-Molina, A.E., Alvarez, M.C., Sierro, F.J., Singh, S.D., Mahanti, S., and Giosan, L., 2014. Sedimentation rates from calcareous nannofossil and planktonic foraminifera biostratigraphy in the Andaman Sea, northern Bay of Bengal, and Eastern Arabian Sea. *Marine and Petroleum Geology* 58, 425–437. <https://doi.org/10.1016/j.marpetgeo.2014.08.011>.
- Garzanti, E., Wang, J.-G., Vezzoli, G., and Limonta, M., 2016. Tracing provenance and sediment fluxes in the Irrawaddy River basin (Myanmar). *Chemical Geology*, 440, 73–90. <https://doi.org/10.1016/j.chemgeo.2016.06.010>.
- Gebregiorgis, D., Hathorne, E.C., Giosan, L., Clemens, S., Nürnberg, D., and Frank, M., 2018. Southern Hemisphere forcing of South Asian monsoon precipitation over the past ~1 million years. *Nature Communications* 9, 4702. [doi.org/10.1038/s41467-018-07076-2](https://doi.org/10.1038/s41467-018-07076-2).
- Giosan, L., Naing, T., Tun, M. M., Clift, P. D., Filip, F., Constantinescu, S., Khonde, N., Blusztajn, J. S., Buylaert, J.-P., and Stevens, T., 2018. On the Holocene evolution of the Ayeyarwady megadelta. *Earth Surface Dynamics* 6, 451–466. [doi.org/10.5194/esurf-6-451-2018](https://doi.org/10.5194/esurf-6-451-2018).
- Gupta, A.K., Yuvaraja, A., Prakasam, M., Clemens, S.C., Velu, A., 2015. Evolution of the South Asian monsoon wind system since the late Middle Miocene. *Palaeogeography, Palaeoclimatology, Palaeoecology* 438, 160–167. [doi.org/10.1016/j.palaeo.2015.08.006](https://doi.org/10.1016/j.palaeo.2015.08.006).
- Hamilton, P., O’Nions, R., Bridgwater, D., Nutman, A., 1983. Sm–Nd studies of Archaean metasediments and metavolcanics from West Greenland and their implications for the Earth’s early history. *Earth and Planetary Science Letters* 62, 263–272. [doi.org/10.1016/0012-821X\(83\)90089-4](https://doi.org/10.1016/0012-821X(83)90089-4).
- Huang, Y., Clemens, S. C., Liu, W., Wang, Y., and Prell, W. L., 2007. Large-scale hydrological change drove the late Miocene C4 plant expansion in the Himalayan foreland and Arabian Peninsula. *Geology*, 35, 531–534. <https://doi.org/10.1130/G23666A.1>.
- Jia, G., Peng, P. A., Zhao, Q., and Jian, Z., 2003. Changes in terrestrial ecosystem since 30 Ma in East Asia: stable isotope evidence from black carbon in the South China Sea. *Geology*, 31, 1093–1096. <https://doi.org/10.1130/G1992.1>.
- Johnson, J.E., Phillips, S.C., Torres, M.E., Piñero, E., Rose, K.K., and Giosan, L., 2014. Influence of total organic carbon deposition on the inventory of gas hydrate in the Indian continental margins. *Marine and Petroleum Geology* 58, 406–424. <https://doi.org/10.1016/j.marpetgeo.2014.08.021>.
- Kurian, S., Nath, B. N., Ramaswamy, V., Naman, D., Rao, T. G., Raju, K. K., Selvaraj, K., and Chen, C., 2008. Possible detrital, diagenetic and hydrothermal sources for Holocene sediments of the Andaman backarc basin. *Marine Geology*, 247, 178–193. <https://doi.org/10.1016/j.margeo.2007.09.006>.
- Li, J., Fang, X., Song, C., Pan, B., Ma, Y., and Yan, M., 2014. Late Miocene–Quaternary rapid stepwise uplift of the NE Tibetan Plateau and its effects on climatic and environmental changes. *Quaternary Research*, 81, 400–423. [doi.org/10.1016/j.yqres.2014.01.002](https://doi.org/10.1016/j.yqres.2014.01.002).
- Li, P., Zhang, C., Guo, Z., Deng, C., Ji, X., Jablonski, N.G., Wu, H., Zhu, R., 2019. Clay mineral assemblages in the Zhaotong Basin of southwestern China: implications for the late Miocene and Pliocene evolution of the South Asian monsoon. *Palaeogeography, Palaeoclimatology, Palaeoecology* 516, 90–100. [doi.org/10.1016/j.palaeo.2018.11.039](https://doi.org/10.1016/j.palaeo.2018.11.039).
- Liew, T., McCulloch, M., 1985. Genesis of granitoid batholiths of Peninsular Malaysia and implications for models of crustal evolution: evidence from a Nd–Sr isotopic and U–Pb zircon study. *Geochimica et Cosmochimica Acta* 49, 587–600. [doi.org/10.1016/0016-7037\(85\)90050-X](https://doi.org/10.1016/0016-7037(85)90050-X).
- Liu, Z., Colin, C., Trentesaux, A., Blamart, D., Bassinot, F., Siani, G., Sicre, M.-A., 2004. Erosional history of the eastern Tibetan Plateau since 190 kyr ago: clay mineralogy and geochemical investigations from the southwestern South China Sea. *Marine Geology* 209, 1–18. <https://doi.org/10.1016/j.margeo.2004.06.004>.
- Liu, J., Yan, W., Chen, Z., Lu, J., 2012. Sediment sources and their contribution along northern coast of the South China Sea: evidence from clay minerals of surface sediments. *Continental Shelf Research* 47, 156–164. [doi.org/10.1016/j.csr.2012.07.013](https://doi.org/10.1016/j.csr.2012.07.013).
- Luhr, J. F., and Haldar, D., 2006. Barren Island Volcano (NE Indian Ocean): island-arc high-alumina basalts produced by troctolite contamination. *Journal of Volcanology and Geothermal Research*, 149, 177–212. <https://doi.org/10.1016/j.jvolgeores.2005.06.003>.
- Miriayala, P., Sukumaran, N.P., Nath, B.N., Ramamurthy, P.B., Sijinkumar, A.V., Vijayagopal, B., Ramaswamy, V., Sebastian, T., 2017. Increased chemical weathering during the deglaciation to mid-Holocene summer monsoon intensification. *Scientific Reports* 7, 44310. [doi.org/10.1038/srep44310](https://doi.org/10.1038/srep44310).
- Moore, D.M., Reynolds, R.C., 1989. *X-ray Diffraction and the Identification and Analysis of Clay Minerals*. Oxford University Press, Oxford (332 pp.).
- Phillips, S.C., Johnson, J.E., Underwood, M.B., Guo, J., Giosan, L., Rose, K., 2014. Long-term scale variation in bulk and clay mineral composition of Indian continental margin sediments in the Bay of Bengal, Arabian Sea, and Andaman Sea. *Marine and Petroleum Geology* 58, 117–138. <https://doi.org/10.1016/j.marpetgeo.2014.06.018>.
- Pin, C., Zalduaguei, J.S., 1997. Sequential separation of light rare-earth elements, thorium and uranium by miniaturized extraction chromatography: application to isotopic analyses of silicate rocks. *Analytica Chimica Acta* 339, 79–89. [doi.org/10.1016/S0003-2670\(96\)00499-0](https://doi.org/10.1016/S0003-2670(96)00499-0).
- Potemra, J.T., Luther, M.E., O’Brien, J.J., 1991. The seasonal circulation of the upper ocean in the Bay of Bengal. *Journal of Geophysical Research Oceans* 96, 12667–12683. <https://doi.org/10.1029/91JC01045>.
- Rao, P., Ramaswamy, V., Thwin, S., 2005. Sediment texture, distribution and transport on the Ayeyarwady continental shelf, Andaman Sea. *Marine Geology* 216, 239–247. <https://doi.org/10.1016/j.margeo.2005.02.016>.
- Rizal, S., Damm, P., Wahid, M.A., Sundermann, J., Ilhamsyah, Y., Iskandar, T., 2012. General circulation in the Malacca Strait and Andaman Sea: a numerical model study. *American Journal of Environmental Sciences* 8, 479. [doi.org/10.3844/ajessp.2012.479.488](https://doi.org/10.3844/ajessp.2012.479.488).
- Robinson, R.A.J., Bird, M., Oo, N.W., Hoey, T., Aye, M.M., Higgitt, D., Swe, A., Tun, T., Win, S.L., 2007. The Irrawaddy river sediment flux to the Indian Ocean: the original nineteenth-century data revisited. *The Journal of Geology* 115, 629–640. <https://doi.org/10.1086/521607>.

- Shen, X., Wan, S., France-Lanord, C., Clift, P.D., Tada, R., Révillon, S., Shi, X., Zhao, D., Liu, Y., Yin, X., 2017. History of Asian eolian input to the Sea of Japan since 15 Ma: links to Tibetan uplift or global cooling? *Earth and Planetary Science Letters* 474, 296–308. doi.org/10.1016/j.epsl.2017.06.053.
- Sijinkumar, A., Clemens, S., Nath, B.N., Prell, W., Benshila, R., Lengaigne, M., 2016.  $\delta^{18}\text{O}$  and salinity variability from the Last Glacial Maximum to Recent in the Bay of Bengal and Andaman Sea. *Quaternary Science Reviews* 135, 79–91. doi.org/10.1016/j.quascirev.2016.01.022.
- Singh, S.C., Moeremans, R., McArdle, J., Johansen, K., 2013. Seismic images of the sliver strike-slip fault and back thrust in the Andaman-Nicobar region. *Journal of Geophysical Research Solid Earth* 118, 5208–5224. <https://doi.org/10.1002/jgrb.50378>.
- Steinke, S., Hanebuth, T.J.J., Vogt, C., Statterger, K., 2008. Sea level induced variations in clay mineral composition in the southwestern South China Sea over the past 17, 000 yr. *Marine Geology*, 250, 199–210. <https://doi.org/10.1016/j.margeo.2008.01.005>.
- Stokke, P.R., Carson, B., 1973. Variation in clay mineral X-ray diffraction results with the quantity of sample mounted. *Journal of Sedimentary Petrology* 43, 957–964.
- Tanaka, T., Togashi, S., Kamioka, H., Amakawa, H., Kagami, H., Hamamoto, T., Yuhara, M., Orihashi, Y., Yoneda, S., Shimizu, H., 2000. JNdi-1: a neodymium isotopic reference in consistency with LaJolla neodymium. *Chemical Geology* 168, 279–281. doi.org/10.1016/S0009-2541(00)00198-4.
- Tripathi, S., Tiwari, M., Lee, J., Khim, B.-K., IODP Expedition 353 Scientists, 2017. First evidence of denitrification vis-à-vis monsoon in the Arabian Sea since Late Miocene. *Scientific Reports* 7, 43056. <https://doi.org/10.1038/srep43056>.
- Wan, S., Clift, P.D., Li, A., Li, T., Yin, X., 2010. Geochemical records in the South China Sea: implications for East Asian summer monsoon evolution over the last 20 Ma. Geological Society, London, Special Publications 342, 245–263. <https://doi.org/10.1144/SP342.14>.
- Wan, S., Yu, Z., Clift, P.D., Sun, H., Li, A., Li, T., 2012. History of Asian eolian input to the West Philippine Sea over the last one million years. *Palaeogeography, Palaeoclimatology, Palaeoecology* 326, 152–159. doi.org/10.1016/j.palaeo.2012.02.015.
- Wang, B., Clemens, S.C., Liu, P., 2003. Contrasting the Indian and East Asian monsoons: implications on geologic timescales. *Marine Geology* 201, 5–21. [https://doi.org/10.1016/S0025-3227\(03\)00196-8](https://doi.org/10.1016/S0025-3227(03)00196-8).
- Webster, P.J., 1987. The elementary monsoon. In: Fein, J.S., Stephens, P.L. (Eds.), *Monsoons*. John Wiley & Sons, New York, pp. 3–32.
- Zachos, J., Pagani, M., Sloan, L., Thomas, E., Billups, K., 2001. Trends, rhythms, and aberrations in global climate 65 Ma to present. *Science* 292, 686–693. doi.org/10.1126/science.1059412.
- Zin-Maung-Maung-Thein, Takai, M., Uno, H., Wynn, J.G., Egi, N., Tsubamoto, T., Nishimura, T., Yoneda, M., 2011. Stable isotope analysis of the tooth enamel of Chaingzauk mammalian fauna (late Neogene, Myanmar) and its implication to paleoenvironment and paleogeography. *Palaeogeography, Palaeoclimatology, Palaeoecology* 300, 11–22. <https://doi.org/10.1016/j.palaeo.2010.11.016>.